

MINI-REVIEW

Measurement of Oxygen Concentrations in the Intact Beating Heart Using Electron Paramagnetic Resonance Spectroscopy: A Technique for Measuring Oxygen Concentrations *In Situ*

Jay L. Zweier,¹ Susan Thompson-Gorman,¹ and Periannan Kuppusamy¹

Received July 5, 1991

Abstract

Electron paramagnetic resonance (EPR) spectroscopy can be applied to measure oxygen concentrations in cells and tissues. Oxygen is paramagnetic, and thus it interacts with a free radical label resulting in a broadening of the observed linewidth. Recently we have developed instrumentation in order to enable the performance of EPR spectroscopy and EPR oximetry in the intact beating heart. This spectrometer consists of 1–2-GHz microwave bridge with the source locked to the resonant frequency of a specially designed lumped circuit resonator. This technique is applied to measure the kinetics of the uptake and clearance of different free radical labels. It is demonstrated that this technique can be used to noninvasively measure tissue oxygen concentration. In addition, rapid scan EPR measurements can be performed enabling gated millisecond measurements of oxygen concentrations to be performed over the cardiac cycle. Thus, low-frequency EPR spectroscopy offers great promise in the study of tissue oxygen concentrations and the role of oxygen in metabolic control.

Key Words: Electron paramagnetic resonance; loop-gap resonator; reperfusion; oximetry.

Introduction

Over the past four decades since the discovery of electron paramagnetic resonance (EPR), spectroscopy advances in microwave source and signal

¹The Electron Paramagnetic Resonance Laboratories, Department of Medicine, Division of Cardiology, The Johns Hopkins Medical Institutions, Francis Scott Key Medical Center, Baltimore, Maryland 21224.

processing technology enabled the development of instrumentation capable of performing sensitive measurements of the free radicals and paramagnetic ions in solids and small chemical samples. As a result, EPR spectroscopy has become an important technique for studying the many chemical reaction mechanisms involving free-radical intermediates. Over the last decade free radicals have been suggested to be important mediators of a wide range of clinical diseases including heart attack, stroke, respiratory distress syndrome, acute tubular necrosis of the kidney, reperfusion injury of a variety of organs, and oncogenesis and tumor promotion (Weisfeldt *et al.*, 1988; Taylor *et al.*, 1986). Even the process of aging itself has been proposed to be due to the formation of reactive oxygen free radicals (Armstrong *et al.*, 1984). Thus, free radicals have been proposed to mediate many of the most prevalent diseases causing morbidity and mortality.

Though EPR spectroscopy has been widely applied to study biological and biochemical problems of isolated proteins and enzymes involving free radicals and paramagnetic metal ions, similar measurements have not been performed in intact biological tissues. Conventional spectrometer designs, which are commercially available, are typically built utilizing microwave frequencies of 8–10 GHz, X-band, or 35–40 GHz, Q-band with standard rectangular or cylindrical resonant cavities. With these spectrometer designs the maximum thickness of the nonfrozen aqueous sample that can be studied is approximately 1 or 0.2 mm, respectively. Thus these designs set a limit on the size of a biological sample which can be measured.

We recently reported the development of an EPR spectrometer designed to enable high-sensitivity EPR measurements of whole biological organs and tissues (Zweier and Kuppusamy, 1988). Using this spectrometer, one can perform measurements of the kinetics of radical label uptake and clearance in the intact beating heart. In this paper we will describe the instrumentation which we have developed and how it can be applied to enable measurements of the EPR spectra of a free-radical label in the beating heart and the determination of oxygen concentrations from these spectral data.

Methods

Loop-Gap Resonator

Lumped circuit resonator designs were described as early as 1940, and recently these resonators have been demonstrated to be useful for application to NMR and EPR spectroscopy (Hardy and Whitehead, 1981; Froncisz and Hyde, 1982). These designs were referred to initially as split-ring resonators, and subsequently the term loop-gap resonator has been coined to encompass a broad range of variations of these designs (Froncisz and Hyde, 1982). The

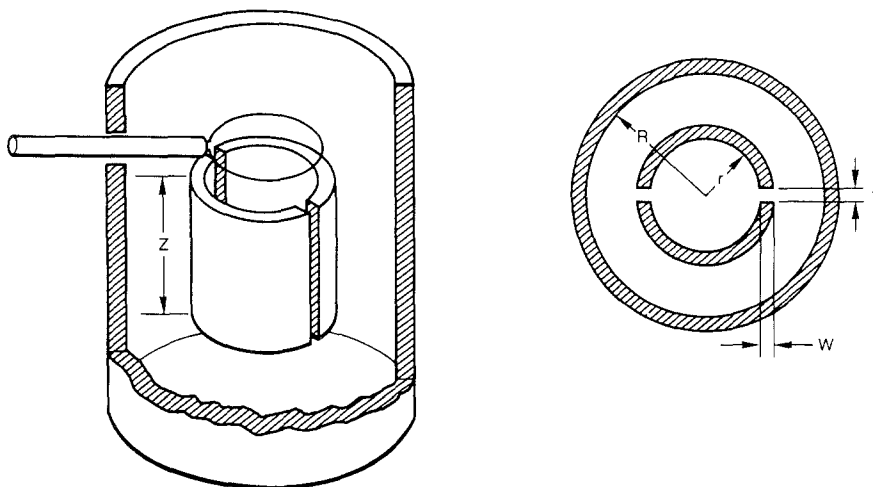


Fig. 1. Schematic diagram of the loop-gap resonator.

split-ring resonator or loop-gap resonator designs which we employ can be visualized as a split conducting cylinder consisting of an inductive ring, or loop, and two air-gap plate capacitors as shown in Fig. 1. The critical dimensions of this resonator include: r , the resonator radius; t , the gap size; w , the width of the capacitive plates; n , the number of gaps; and z , the resonator length. This resonator is placed within a conducting shield of radius R , which must be less than the cutoff wavelength for the lowest excited propagational mode of cylindrical waveguide in order to suppress the external radiation of microwave energy which is observed when the resonator dimensions approach quarter wavelength. Coupling of microwave power is achieved via an inductive coupling loop. To a first approximation the loop-gap resonator can be considered as a simple inductance and capacitance lumped circuit (Froncisz and Hyde, 1982).

Loop-gap resonators are superior to conventional cavity resonators for accommodating large aqueous samples based on the fact that the maximum E field is localized within the gap and the maximum H field is localized in the bore. Thus, maximum H field and minimum E are observed at a sample in the center of the resonator bore minimizing the loss in resonator Q observed from loading with a lossy dielectric aqueous sample. Therefore, relatively high Q values can be observed in the presence of high filling factors, enabling high sensitivity to be obtained in EPR applications. The maximum attainable sensitivity for EPR measurements performed at any given frequency is

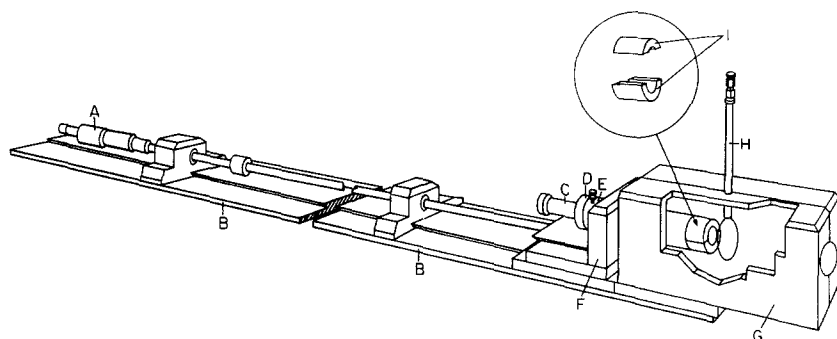


Fig. 2. Diagram of the loop-gap resonator design used for studies of intact biological tissues. The labeled parts include: (A) coupling adjustment micrometer; (B) support rail; (C) sample tube; (D) sample tube holder; (E) resonator support rod; (F) spring-loaded resonator coupling adjustment stage; (G) shield; (H) semirigid coax coupling loop; (I) resonator halves. The outer shield, G, is shown partially peeled open in order to illustrate the resonator and coupling loop within.

defined as (Feher, 1957; Poole, 1967)

$$C_{\min} = K/Q_u \eta \omega_0^2 (P_w)^{1/2} \quad (1)$$

where C_{\min} is the minimum detectable radical concentration, Q_u is the unloaded Q of the resonator, η is the filling factor, ω_0 is the microwave frequency, P_w is the applied microwave power, and K is a frequency-independent constant. Thus, maximum sensitivity is obtained when the filling factor, the Q , and the resonance frequency are maximized.

A rugged versatile resonator design was constructed suitable for *in vivo* tissue EPR applications. As shown in Fig. 2, this resonator design consists of an outer shield with $R = 2.06$ cm, an inner loop-gap resonator insert rod, the resonator halves which attach to the insert rod, a coupling loop, and a mechanical micrometer-controlled stage used to precisely move the resonator with respect to the coupling loop. The shield was machined from rexolite plastic blocks, and a series of resonator inserts and resonator halves were also machined from rexolite. The shield was silvered with a $10 \mu\text{m}$ thickness of silver deposited by ion beam deposition. The resonator halves were coated with pure 99.9% silver foil which was attached to the plastic using transfer adhesive. For optimum performance in EPR applications with maximum Q , the silvered conducting surface of the resonator must be at least 10 times the microwave frequency skin depth. However, in order to achieve adequate field modulation penetration at frequencies of 50 or 100 kHz, the thickness cannot exceed 25–50 μm . Therefore, the resonator was silvered with a foil of 25 μm in thickness. The coupling loop consisted of a short length of 3-mm-diameter

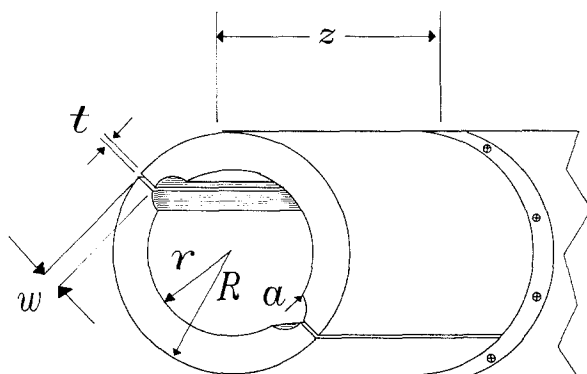


Fig. 3. Diagram of the recessed loop-gap resonator used in the studies of intact hearts. The gaps are recessed by a semicylindrical hole of radius a .

semirigid coax with inner conductor looped and soldered to the outer conductor. Coupling of microwave power was varied by moving the resonator with respect to the coupling loop, with precise movement achieved using the micrometer-controlled stage.

Recessed Loop-Gap Resonator

In order to accommodate aqueous sample sizes as large as 10–20 mm diameter, the resonant frequency must be in the range of 1–2 GHz, L-band or below. An optimum (filling factor $\times Q$) product was observed for aqueous samples of 13–15 mm diameter with resonator dimensions $r = 13$ mm, $t = 0.25$ mm, $w = 3$ mm, $n = 2$, and $z = 25$ mm. The resonant frequency of this resonator was 1.1 GHz with an unloaded Q of 2,000. The Q dropped to 600 when the resonator was filled with a 13-mm aqueous sample. It was observed that the Q of the sample-containing resonator could be further increased by recessing the gaps with semicylindrical holes (Fig. 3). Recessing the gaps has the effect of decreasing E fringe field at the sample, decreasing dielectric loss, and increasing resonator Q with only a small effective decrease in resonator filling factor. The recessed loop-gap resonator with the above dimensions and with recession radius $a = 4$ mm at a resonant frequency of 1.1 GHz had a Q of 1,000 when loaded with a 13-mm-diameter aqueous sample. Field modulation was achieved with 8-cm-diameter, 100-turn modulation coils mounted on the side walls of the resonator shield. These large modulation coils were tuned with an external capacitance box in order to maximize the field modulation. The modulation amplitude and signal phase were calibrated with a point sample of diphenylpicrylhydrazyl (DPPH) radical placed in a 5-mm tube within the resonator. The Bruker ESP 300 computer calibration program was used to automatically calibrate amplitude and

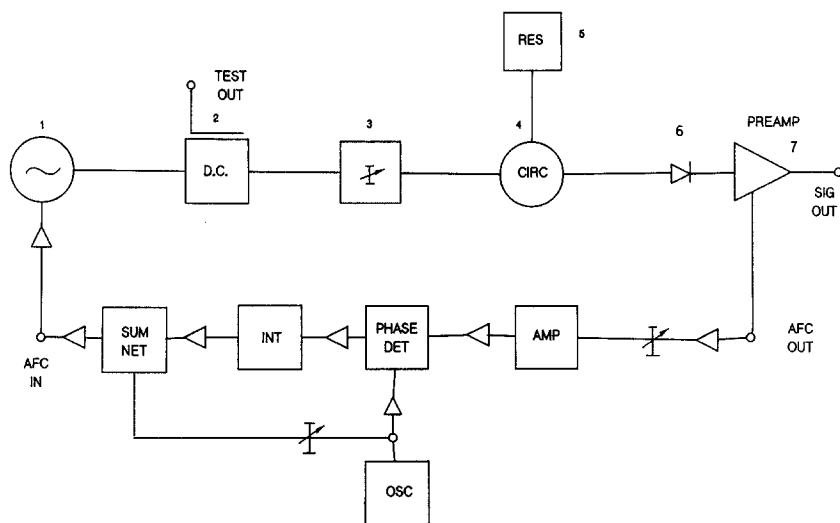


Fig. 4. Block diagram of the L-band microwave bridge. The top line shows the microwave components: (1) cavity-stabilized 1-2-GHz transistor oscillator; (2) directional coupler with test port connected to a microwave frequency counter; (3) variable attenuator with a 60-dB range; (4) three-port L-band circulator; (5) resonator; (6) Schotky diode detector; (7) preamplifier stage with the output connected to the input of the Bruker signal channel lock-in amplifier. The bottom line illustrates the AFC feedback loop used to lock the oscillator to the resonant frequency of the resonator.

phase. The values obtained were verified to be correct with manual measurements. Maximum modulation amplitudes of 0.5 G were obtained at 100 kHz and amplitudes of greater than 1.0 G at 50, 25 and 12.5 kHz.

Resonators were tested using an EIP 935 or Wavetek 2005 microwave sweeper. Measurements of resonant frequency Q and H_1 fields were also performed. Unloaded Q was measured as twice the resonance width at half power absorption with the resonator critically coupled. The H_1 field values were measured with either a cylindrical or spherical piece of copper as described previously (Freed *et al.*, 1967).

L-band Microwave Bridge

The L-band microwave bridge consisted of a cavity-stabilized transistor oscillator as the frequency source. This oscillator tuned the frequency range of 1-2 GHz with a maximum power output of approximately 100 mW. The block diagram shown in Fig. 4 illustrates the components of the bridge. The oscillator was locked to the resonant frequency of the sample resonator using an AFC feedback loop. Port 2 of the circulator of the microwave bridge was

connected to the loop-gap resonator, and the directional coupler test port was connected to an EIP microwave frequency counter.

Heart Preparation

Isolated rat hearts were perfused by the method of Langendorff using a Krebs/bicarbonate buffered perfusate consisting of 117 mM NaCl, 24.6 mM NaHCO_3 , 5.9 mM KCl, 1.2 mM MgCl_2 , 2.0 mM CaCl_2 , and 16.7 mM glucose bubbled with 95% O_2 /5% CO_2 as described previously (Zweier and Jacobus, 1989). The perfusate solutions were filtered through 0.8- μM millipore filters prior to use. Heart rate and left ventricular developed pressure were measured using a fluid-filled balloon secured into the left ventricle. The balloon was connected to a Statham P23 DB pressure transducer via a hydraulic line and the transducer output amplified to a strip chart recorder. The ventricular volume was adjusted to achieve a left ventricular end diastolic pressure of 12 mm Hg.

Results

Sensitivity

The sensitivity of the spectrometer with the recessed loop-gap resonator was evaluated using an aqueous solution of TEMPO (2,2,6,6-tetramethylpiperidinyloxy) free radical. Sample tubes of 13 and 15 mm were studied with sample volumes of 1–2 ml. As shown in Fig. 5A, with 2-min spectral acquisitions, signal-to-noise ratios of greater than 1200 were obtained on 1.0 mM solutions of TEMPO spin label, and with a radical concentration of only 2 μM a signal-to-noise ratio greater than 5 was observed (Fig. 5B). Thus, in aqueous solutions a concentration of as low as 0.4 μM was detectable.

Studies with Perfused Heart

Hearts were removed from 200-g rats and perfused in a Langendorff mode with a constant coronary flow of 10 ml/min, yielding a perfusion pressure of approximately 80 mm Hg. A left ventricular balloon was inserted from the left atrium to the left ventricle to enable continuous measurement of left ventricular pressure and heart rate. The hearts were then placed in 13-mm tubes and the tube placed within the bore of the recessed loop-gap resonator (Fig. 6). A drainage catheter inserted at the bottom of the tube and connected to an aspiration pump removed continuously all the perfusate solution from and around the heart, preventing flooding of the resonator. This also enabled measurements of radical uptake and clearance from the heart, eliminating the problem of an effluent-perfusate signal. The microwave

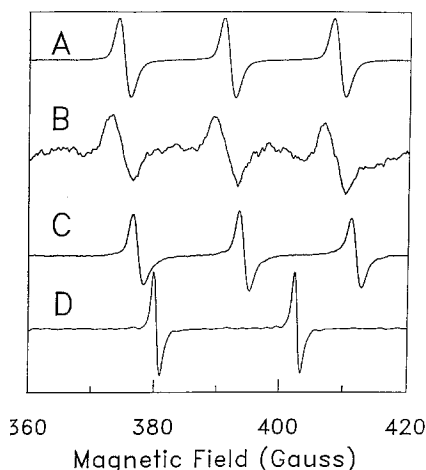


Fig. 5. (A) EPR spectrum of an aqueous 1.0 mM TEMPO solution filling a 13-mm cylindrical tube. The resonant frequency is 1.085 GHz with a modulation amplitude of 0.5 G, modulation frequency of 50 kHz, microwave power of 100 mW, and acquisition time of 2 min. (B) EPR spectrum of an aqueous 2 μ M TEMPO solution filling a 13-mm cylindrical tube. The spectrum was acquired as described for spectrum A. (C) EPR spectrum of a perfused rat heart in a 13-mm tube. The heart was perfused with a solution containing 1.0 mM TEMPO. A 2-min acquisition was obtained 5 min after starting the radical infusion. (D) EPR spectrum of heart perfused with 1 mM ^{15}N -PDT. The scan time was 30 sec.

bridge AFC loop made it possible to minimize any frequency noise which resulted from the motion of the beating heart. Control spectra, prior to infusion of spin labels, showed no EPR signal.

Infusion of 1.0 mM TEMPO or ^{15}N -PDT (perdeuterated TEMPONE, 4-oxo-2,2,6,6-tetramethylpiperidine- d_{16} , 1- ^{15}N -1-oxyl) free radical with the perfusate solution was followed by repetitive EPR acquisitions for 30 min. Infusion of the radical was then stopped and repetitive spectra acquired to measure the kinetics of radical clearance. The left ventricular developed pressure of these hearts was approximately 120 mm Hg with a fixed diastolic pressure of 12 mm Hg and an intrinsic heart rate of 200–250 bpm. Infusion of the radicals had no effect on contractile function or heart rate. Immediately after the start of the infusion, the prominent triplet TEMPO signal (Fig. 5C) or doublet ^{15}N -PDT signal (Fig. 5D) was clearly seen with signal-to-noise ratios of greater than 400 or 600, respectively. In the case of TEMPO, the intensity of the signal increased rapidly over the first five minutes of infusion with a half maximum after 2 min followed by a further gradual increase over the next 10 min of administration as seen in Fig. 7. A similar behavior was seen in the case of ^{15}N -PDT infusion except that the half maximum was at less than 1 min (Fig. 7). At the end of 30 min, i.e., when the signal intensity

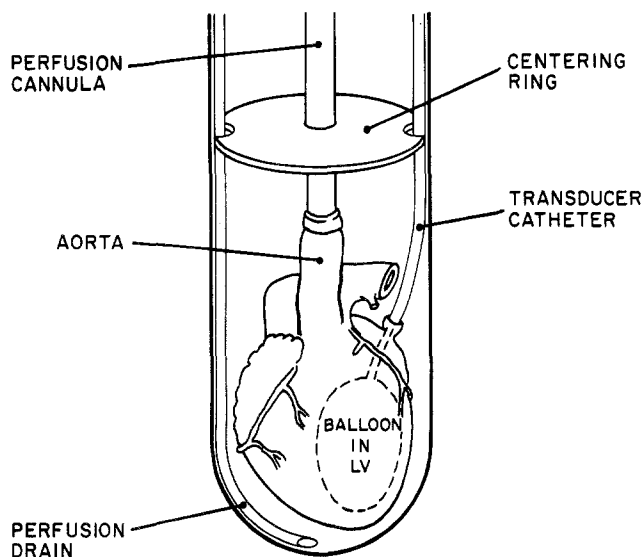


Fig. 6. Diagram of perfused heart preparation.

reached a steady state, the infusion of radical was stopped while the spectral acquisitions were continued for another 30 min to follow the radical clearance from the heart. A rapid decay of the signal was observed with both the spin labels (Fig. 7).

In order to get an understanding of the nature and rate of radical uptake and clearance, we analyzed the observed intensity data using standard fitting routines. As shown in Fig. 7 the time course of radical uptake could be precisely modeled as a first-order process with a rate constant $k = 0.85 \pm 0.05 \text{ min}^{-1}$ for TEMPO and $k = 1.12 \pm 0.06 \text{ min}^{-1}$ for ^{15}N -PDT. Clearance of the radical from the heart after termination of infusion was observed to proceed in more than a single phase. A single exponential function was not sufficient to fit the observed data satisfactorily. A plot of $\log(\text{intensity})$ vs. time showed clearly the involvement of two processes as shown in the insets of Figs. 8 and 9. Therefore, the data were fitted with a linear combination of two exponentials, which yielded the rate constants for the two processes. In the case of TEMPO, the rate constants of clearance were 2.2 ± 0.2 and $0.40 \pm 0.04 \text{ min}^{-1}$. The faster process accounted for about 65% of the radical loss, while the slower process accounted for 35%. The rate constants for the clearance of ^{15}N -PDT radicals in the perfused heart were found to be 4.47 ± 0.27 and $0.44 \pm 0.09 \text{ min}^{-1}$ with the faster process accounting for 84% of the radical loss while that of the slower process being 16%. The faster

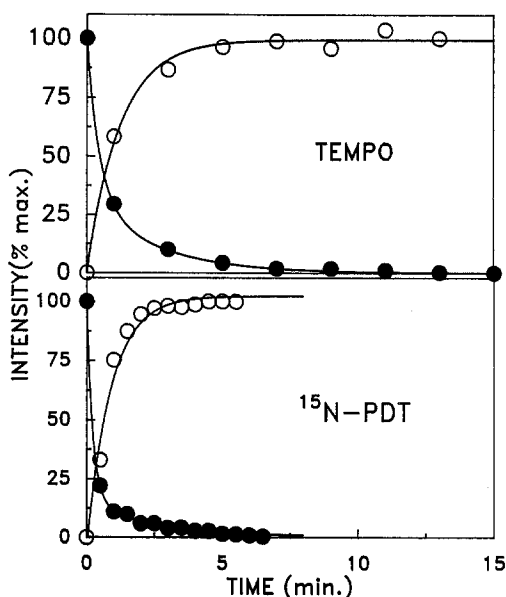


Fig. 7. Graph of the kinetics of radical uptake (O) and clearance (●) in the isolated perfused heart (Top, TEMPO; bottom, ^{15}N -PDT). For measurements of radical uptake (O), hearts were perfused with 1.0 mM spin label starting at time 0, and repetitive 2-min (TEMPO) or 0.5-min (^{15}N -PDT) EPR acquisitions of 100 G (TEMPO) or 60 G (^{15}N -PDT) sweep were performed and the signal intensity was determined from double integration of the signal. The kinetic data were fitted with a single exponential with rate constant $k = 0.85 \text{ min}^{-1}$ for TEMPO and $k = 1.12 \text{ min}^{-1}$ for ^{15}N -PDT. For measurement of radical clearance (●), radical infusion was stopped after 30 min at time 0, and repetitive 2-min acquisitions performed. The process of radical clearance proceeded in 2 phases requiring fitting with a linear combination of two exponentials. For TEMPO, the rate constants were $k = 2.2 \text{ min}^{-1}$ (weight 65%) and $k = 0.4 \text{ min}^{-1}$ (weight 35%). For ^{15}N -PDT, the rate constants were $k = 4.47 \text{ min}^{-1}$ (weight 84%) and $k = 0.44 \text{ min}^{-1}$ (weight 16%).

process probably represents the vascular washout while the slower process may be due to cellular enzyme reduction.

Studies with Ischemic Heart

Hearts were perfused with 1.0 mM spin label as described above for 30 min and then subjected to global ischemia with perfusion stopped. Repetitive EPR acquisitions were then performed for 30 min. Unlike radical clearance in the perfused heart, a gradual decrease in radical concentrations was observed in the ischemic heart. The kinetic data could be precisely fitted with a single first-order exponential with rate constant of $0.40 \pm 0.01 \text{ min}^{-1}$ for TEMPO (Fig. 8) and $0.37 \pm 0.03 \text{ min}^{-1}$ for ^{15}N -PDT (Fig. 9). The observed

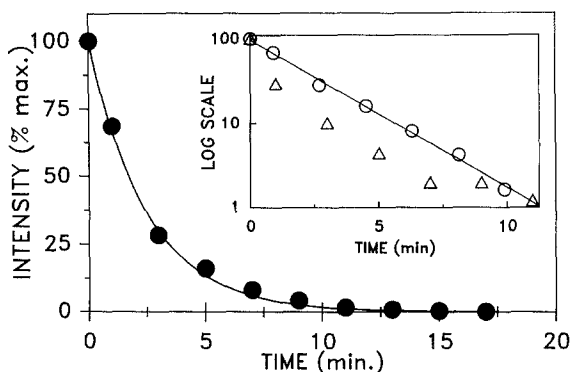


Fig. 8. Graph of the kinetics of free radical metabolism in the ischemic heart. The heart was loaded with a 30-min infusion of 1.0 mM TEMPO followed by induction of ischemia at time 0. Measurements were performed as described in Fig. 7. The kinetic data of radical decay were fitted with a single exponential with rate constant $k = 0.40 \text{ min}^{-1}$. (Inset) Semilogarithmic plot of decay (O) is linear. Also shown for comparison are decay data (Δ) of the heart perfused with TEMPO which is nonlinear and required two functions for fitting.

rate constants correspond closely to that of the respective slower process observed during radical clearance of the normally perfused heart.

EPR Oximetry

Molecular oxygen is paramagnetic and exists in the triplet ground state with spin $S = 1$. In solution it can undergo Heisenberg exchange interaction

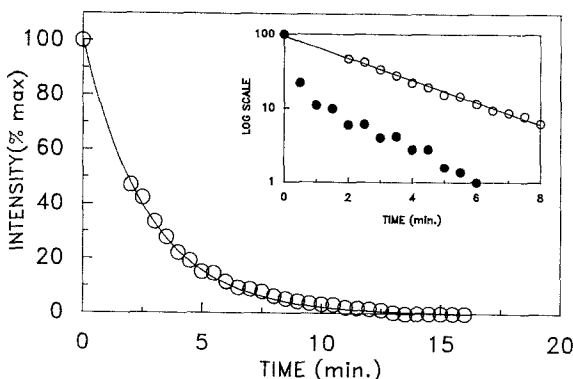


Fig. 9. Graph of the kinetics of free-radical metabolism in the ischemic heart. The heart was loaded with a 30-min infusion of 1.0 mM ^{15}N -PDT followed by induction of ischemia at time 0. Measurements were performed as described in Fig. 7. The kinetic data of radical decay were fitted with a single exponential with rate constant $k = 0.37 \text{ min}^{-1}$. (Inset) Semilogarithmic plot of decay (O) is linear. Also shown for comparison are decay data (\bullet) of the heart perfused with TEMPO which is nonlinear and required two functions for fitting.

with other paramagnetic species, like the spin label TEMPO, and this will result in a broadening of the observed EPR line. The magnitude of this broadening depends on the exchange rate ω , which in turn is governed by the Smoluchowski equation:

$$\omega = 4\pi R \{D(\text{O}_2) + D(\text{TEMPO})\} [\text{O}_2] \quad (2)$$

where R is the interaction distance between oxygen and the spin label, which is generally assumed to be 4.5 Å, $D(\text{O}_2)$ and $D(\text{TEMPO})$ are, respectively, the diffusion constants of oxygen and TEMPO, and $[\text{O}_2]$ is the concentration of oxygen. Normally in aqueous solutions $D(\text{TEMPO})$ is much smaller compared to $D(\text{O}_2)$ and so can be omitted. The exchange rate ω is related to the observed peak-to-peak width of a Lorentzian EPR derivative line, $H_{\text{p-p}}$, as

$$\omega = \frac{\sqrt{3}}{2} \gamma H_{\text{p-p}} \quad (3)$$

where γ is the gyromagnetic ratio. Combining Eqs. (2) and (3), we get

$$H_{\text{p-p}} = \frac{8\pi R}{\sqrt{3}\gamma} D(\text{O}_2)[\text{O}_2] \quad (4)$$

If H is the observed broadening due to paramagnetic oxygen, then we write

$$\Delta H = \frac{8\pi R}{\sqrt{3}\gamma} D(\text{O}_2)[\text{O}_2] \quad (5)$$

The above equation allows one to compute the $[\text{O}_2]$ from the measured EPR line width changes and hence serves as a form of EPR spin-label oximetry.

In our experiments we carefully measured the line width in normally perfused hearts and the line width changes observed during ischemia. During normal perfusion with TEMPO the line width remained invariant at 1.73 ± 0.02 G. This value did not change during the washout of the spin label, even when the spin label concentration decreased by a factor of 10. However, after the induction of ischemia the width of the line gradually decreased and the line continued to sharpen with increasing duration of ischemia. This is in accordance with the decrease in oxygen concentration which would be expected to occur in ischemic myocardium. A maximum line width change of 0.40 G was observed with TEMPO after 20 min of ischemia, after which either the change was insignificant or the line intensity was too low to get a precise estimate for the line width.

The oxygen concentration estimated using the observed line width data and the values are shown in Fig. 10. The oxygen concentration falls off very rapidly from a base value of 500 μM to 240 μM , the concentration of oxygen in air, in less than a minute, and in about 10 min the value approaches

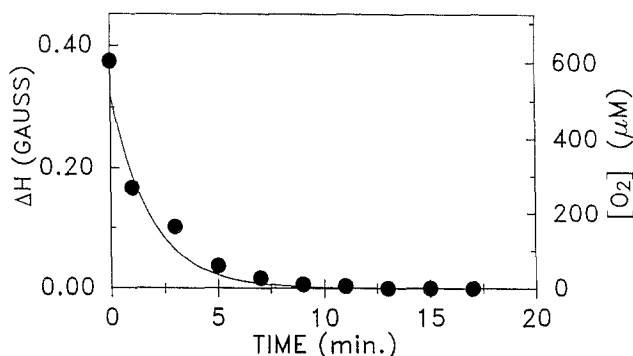


Fig. 10. Graph of myocardial oxygen concentrations in the ischemic heart as a function of the duration of ischemia. Oxygen concentration was calculated from the measured EPR linewidths. EPR measurements were performed as described in Figs. 7 and 8. The kinetics of oxygen consumption were modeled with a single exponential function $k = 0.54 \text{ min}^{-1}$.

zero. Fitting the data with a single exponential model gave a value of $0.54 \pm 0.04 \text{ min}^{-1}$ as the rate constant for oxygen consumption during ischemia.

Instrumentation was developed for the performance of rapid (1–20 msec) gated EPR spectra in the intact beating heart in order to measure the presence and magnitude of alterations in oxygen concentrations which occur during the cardiac cycle. Rapid-scan EPR spectra were obtained using a set of rapid-scan coils mounted on the magnet pole pieces. Field sweep was obtained by driving these coils with a ramp-function generator. A Grass stimulator was used to stimulate cardiac contraction at a frequency of 5 Hz (300 beats/min). A TTL pulse from the stimulator activated the EPR acquisition which, in turn, activated the ramp-generated field sweep at a frequency of 50 Hz, providing 10 EPR measurements per cardiac cycle. In order to increase the signal-to-noise ratio, averaging of 300 cardiac cycles was performed for a total acquisition time of 60 sec.

The hearts were loaded with the spin label ^{15}N -PDT for approximately 5 min, and then gated rapid-scan spectra were measured during continued infusion. With the heart paced at a rate of 300/min, the left ventricular developed pressure was 120 mm Hg and the EPR linewidth was observed to decrease from a baseline value of 741 mG prior to contraction to a minimum of 695 mG at end systole (Fig. 11). During infusion, much of the ^{15}N -PDT spin label will be present in the vascular space. Therefore, in an effort to obtain a more accurate assessment of intracellular oxygen concentrations, the measurements were repeated after stopping infusion for more than 10 sec. The extracellular volume of the 0.5-g rat hearts studied is approximately 0.3 ml so that 10 sec after cessation of infusion with a coronary flow rate of

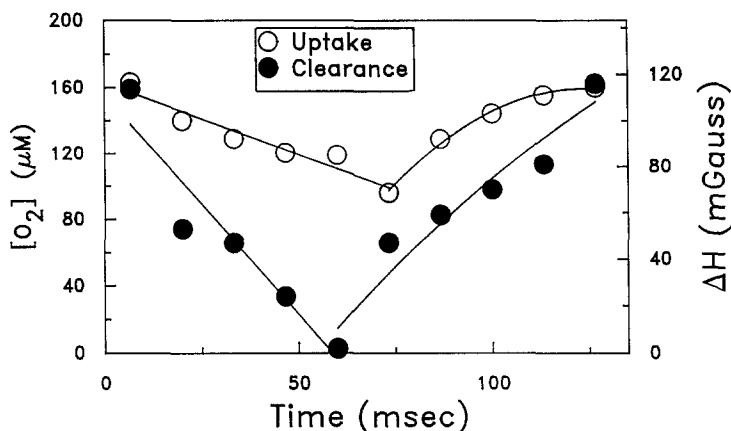


Fig. 11. Gated rapid scan EPR measurements of the linewidth of the ^{15}N -PDT radical label in a beating rat heart, heart rate 300 beats per min. The change in linewidth is shown on the right axis, and the calculated oxygen concentration on the left axis.

10 ml/min most of the vascular and extracellular label would be cleared. In these spectra a narrower baseline linewidth of 638 mG was observed, and it decreased to 502 mG at end systole (Fig. 11).

The O_2 concentration was calculated from the observed linewidth changes. A marked decrease in myocardial oxygen concentration was observed during systole from a maximum of 193 mM to a minimum of 10 mM (Fig. 11). This decrease in O_2 tension coincided with the onset of contraction, with the minimum O_2 concentration observed at end systole and the maximum O_2 concentration at end diastole.

Discussion

Free radicals have been proposed to be important mediators of cell injury in a number of organs and tissues. Recently it has been demonstrated that free radicals are generated in 0.1–1 μM concentrations on reperfusion of ischemic tissues (Zweier, 1988; Zweier *et al.*, 1987). We have demonstrated that high-sensitivity EPR measurements can be performed on intact biological tissues using an L-band microwave bridge with a loop-gap resonator design. This *in vivo* EPR technique was applied to measure the kinetics of free-radical uptake and clearance in the perfused heart. High-quality measurements were obtainable with short acquisition times, enabling precise measurements and modeling. It was demonstrated that the uptake of the TEMPO or ^{15}N -PDT radical could be accurately modeled as a first-order process. Clearance of the radical on termination of infusion, however, was more complex, consisting of

two distinct processes with different rate constants. In the ischemic heart the free-radical signal decreased as a function of time, and the decay of the radicals was precisely modeled as a simple first-order process. Since in the ischemic organ there is no washout, the loss of signal must be solely due to metabolism of the radical. The additional rapid process of radical clearance observed in the perfused heart is presumably due to vascular washout. The slower process of EPR signal decay which was observed in both normally perfused and ischemic hearts is probably due to enzyme reduction of the radical.

It is well known that nitroxide radicals are reduced by cells and biological tissues. Cellular reduction of nitroxide radicals has been one of the major problems encountered in applying spin labeling and spin trapping techniques to the study of cells (Samuni *et al.*, 1986). Lack of knowledge regarding the rate of cellular breakdown of spin-trap adducts has made it difficult to accurately determine the actual rate of radical generation in cells and tissues, since the observed concentration of spin-trap adducts or other radicals is modulated by the rate of radical generation as well as the rate of radical destruction. Thus, measurements of the rate of cellular radical metabolism in whole biological tissues are of critical importance in understanding and characterizing the mechanisms of biological free-radical generation.

All biological tissues consume oxygen, and this process of oxygen consumption is of crucial importance in supplying the energy needs of cells and tissues. In the heart 90% of the ATP generated is derived from mitochondrial oxidative phosphorylation, with the energy required for the generation of ATP derived from the four-electron reduction of molecular oxygen to water (Kobayashi and Neely, 1979). Incomplete reduction of O_2 results in the formation of the superoxide anion radical $\cdot O_2^-$, hydrogen peroxide H_2O_2 , and the hydroxyl radical $\cdot OH$ which are important mediators of cellular oxidative injury. Therefore, the process of O_2 consumption is of great importance in the normal metabolism and the pathology of biological organs and tissues. We have demonstrated that EPR spectroscopy can be applied to noninvasively measure cellular O_2 consumption in the isovolumic beating heart. The consumption of O_2 in the ischemic heart is shown to proceed with a first rate constant of 0.54 min^{-1} . This EPR technique can be similarly applied to other organs and tissues. Measurements of the mean oxygen concentration within the organ can be performed without mechanical perturbation of the tissue as would occur with oxygen electrode techniques. The low, less than mM, concentrations of nitroxide radical required did not have any detectable effect on cardiac function. EPR oximetry has the unique property of targeting the specific area of distribution of the nitroxide radical used. Thus, this technique could be applied to specifically measure oxygen concentrations in different cellular locations within whole biological tissues.

For example, the O_2 concentration adjacent to cell membranes could be distinguished from the concentration within the cell via the use of lipophilic radical probes that would localize within cellular membranes, and hydrophilic probes that would localize in the cytosol. Thus, EPR oximetry can potentially provide information which cannot be obtained with other techniques. In order to fully exploit this property, it will be necessary in the future to develop new free-radical labels which specifically localize to different cellular sites. The technique of performing real-time measurements of oxygen consumption and free-radical generation or metabolism along with simultaneous measurements of contractile function is a unique and powerful method of studying free radical biology and its physiological and pathological effects on the heart.

These techniques which have been developed and applied to study the heart can be similarly applied to other biological organs and tissues. Compared to other biological organs, the heart is relatively difficult to study with EPR spectroscopy due to its mobility and change of shape as a function of the cardiac cycle. In addition, the hollow chambers of the heart decrease the efficiency of resonator filling. Therefore, in other biological tissues it should be possible to attain sensitivities equal to or greater than those we have observed for the heart.

Thus, EPR spectroscopy can be applied to measure free radicals in whole biological organs and tissues. This technique is nondestructive and thus enables the simultaneous measurement of free-radical concentrations and organ function. In addition, rapid measurements of tissue oxygen concentrations can be simultaneously performed over the cardiac cycle. Thus, low-frequency EPR spectroscopy offers great promise in the measurement and assessment of myocardial metabolism.

Acknowledgment

This work was supported by National Institutes of Health Grants HL-17655-13 and HL-38324 and the Squibb American Heart Association Clinician Scientist Award.

References

- Armstrong, D., Sohal, R. S., Cutler, R. G., and Slater, T. F. (1984). Free Radicals in Molecular Biology, Aging and Disease, in *Aging*, Vol. 27, Raven Press, New York.
- Feher, G. (1957). *Bell System Tech. J.* **36**, 449-460.
- Freed, J. H., Leniart, D. S., and Hyde, J. S. (1967). Theory of Saturation and Double Resonance Effects in ESR Spectra. III. RF Coherence and Line Shapes, *J. Chem. Phys.* **47**, 2762-2773.
- Francisz, W., and Hyde, J. S. (1982). The Loop-Gap resonator: A New Microwave Lumped Circuit ESR Sample Structure, *J. Magn. Res.* **47**, 515-521.

- Hardy, W. N., Whitehead, L. A. (1981). Split-Ring Resonator for Use in Magnetic Resonance from 200–2000 MHz, *Rev. Sci. Instrum.* **52**, 213–216.
- Kobayashi, K., and Neely, J. R. (1979) *Circ. Res.* **44**, 166–175.
- Poole, C. P. (1967). *Electron Spin Resonance: A Comprehensive Treatise on Experimental Techniques*, Interscience Publishers, New York, pp. 523–595.
- Samuni, A., Carmichael, A. J., Russo, A., Mitchell, J. B., and Riesz, P. (1986). On the Spin Trapping and ESR Detection of Oxygen-Derived Radicals Generated inside Cells, *Proc. Natl. Acad. Sci. USA* **83**, 7593–7597.
- Taylor, A. E., Matalon, S., and Ward, P. A., eds. (1986). *Physiology of Oxygen Radicals*, Williams and Wilkins, Baltimore.
- Weisfeldt, M. L., Zweier, J. L., and Flaherty, J. T. (1988). Oxygen-derived free radicals and myocardial ischemic injury, in *Heart Disease: Update* (Braunwald, E., ed.), W. B. Saunders, New York, pp. 60–72.
- Zweier, J. L. (1988). Measurement of Superoxide-Derived Free Radicals in the reperfused Heart: Evidence for a Free Radical Mechanism of Reperfusion Injury, *J. Biol. Chem.* **263**, 1353–1357.
- Zweier, J. L., Jacobus, W. E. (1987). Substrate-Induced Alterations of High-Energy Phosphate Metabolism and Contractile Function in the Perfused Heart, *J. Biol. Chem.* **262**, 8015–8021.
- Zweier, J. L., and Kuppusamy, P. (1988). Electron Paramagnetic Resonance Measurements of Free Radicals in the Intact Beating Heart: A Technique for Detection and Characterization of Free Radicals in Whole Biological tissues, *Proc. Natl. Acad. Sci. USA* **85**, 5703–5707.
- Zweier, J. L., Flaherty J. T., and Weisfeldt, M. L. (1987). Direct Measurement of Free Radical generation following Reperfusion of Ischemic Myocardium, *Proc. Natl. Acad. Sci. USA* **84**, 1404–1407.